Chapter 3

Estimating Interval Velocities

In Chapter 2, I showed how the average slowness of the medium can be obtained following migration by a preliminary slowness model. The reason for obtaining average slownesses first is that the curvature in the image of a reflector in a post-migration CRG is affected by all slowness errors above that reflector. These average slownesses are, however, related to the interval slownesses. This chapter discusses obtaining the interval-slowness model (or interval-velocity model) from the average slownesses. This interval-velocity model is what we need to migrate the data.

3.1 LAYER STRIPPING

For one layer, the interval slowness is the same as the average slowness. Therefore, if the method is applied to the top layer only, the interval slowness of that layer will be obtained. When the interval slowness of that layer is known, it can be stripped from the medium when estimating the average slowness of the material below. The process is repeated for the other layers; the top layer is always stripped after its slowness has been determined.

This scheme has two limitations. First, it assumes that the medium is layered. Second, it requires human interaction rendering analysis of a large number of layers tedious. In the rest of this chapter, I will discuss schemes that do not have these limitations.

The idea of layer stripping is, however, a useful concept that can simplify the analysis and make it cheaper. Suppose the velocity down to a given depth is known, either by an independent measurement or by the iterative method presented here. In this case, the portion of the medium down to that depth can be excluded from the velocity analysis. The data need to be downward continued to that depth just once. This stripping can be

done regardless of whether the stripped region is homogeneous or not. All that is assumed is that the velocity down to that depth is known.

3.2 OBTAINING INTERVAL VELOCITIES FROM AVERAGE VELOCITIES

Assuming the depth axis is sampled uniformly, the average slowness at the j-th layer is

$$\bar{w}_j = \frac{\sum_{i=1}^{i=j} w_i}{j} , \tag{3.1}$$

where w_i is the interval slowness of the i-th layer. The inverse of (3.1) is obtaining interval slownesses from average slownesses. The interval slowness, w_i, is obtained from the average slownesses at the top and bottom of that layer,

$$w_i = i\bar{w}_i - (i-1)\bar{w}_{i-1} . \tag{3.2}$$

In Chapter 2, average slownesses were obtained after migration by equation (2.17),

$$\bar{w} = \gamma \bar{w}_m . \tag{3.3}$$

We can, therefore, use equation (3.2) to obtain interval slownesses after obtaining average slownesses from equation (3.3). One problem with equation (3.2) is its great sensitivity in obtaining interval slownesses directly from average slownesses. The reason for this sensitivity is that in equation (3.2) the difference between two quantities is taken, magnifying the errors of those quantities. The problem becomes worse at greater depths because the error in average slownesses is magnified by multiplication by i or $(i-1)$ in equation (3.2). Doing the inverse—calculating average slownesses from interval slownesses—requires summation and is more tolerant to error. If interval slownesses were obtained directly from equation (3.2), they would have wild and unrealistic fluctuations. These fluctuations cannot be simply smoothed because they are unrealistic to start with. Another problem with equation (3.2) is that some γ's may belong to multiples or coherent noise. The average slownesses they give will also result in unreasonable values for the interval slownesses.

These problems are similar to the problems of obtaining interval velocities from stacking

velocities in conventional velocity analysis. To solve these problems in conventional velocity analysis, Toldi (1985) proposed a method in which the model is perturbed using the gradient of an objective function. The gradient is calculated at the current model position and requires calculating the derivative of the objective function in the stacking-velocity space.

In Toldi's scheme, knowing the position of the model in the interval-velocity space implies knowing its position in the stacking-velocity space, because the two spaces are related via the Dix equation. In the scheme presented here, the space that I search ($g(\tau,\gamma)$ in equation (2.7)) is a residual-velocity space in which the current model position is unknown, since knowing the residual velocities implies knowing the true velocities, thereby signaling the end of the search! On the other hand, here I know the *final* model position in the residual velocity space; it lies on the curve $\gamma(z) = 1$ as shown in Figure 3.1b. We can compute the gradient at this position (the light line in Figure 3.1b) and march till we find the current model position in the residual velocity space (the heavy line in Figure 3.1b). This position gives us the error in the initial velocity model we used in migration, thus enabling us to modify the model.

While we are searching in the residual velocity panel, our goal is to bring the curve $\gamma(z)$ as close as possible to the peaks without violating any constraint on the model. The objective function, Γ, that we want to maximize is therefore the sum of the semblances along the that curve. That is,

$$\Gamma = \sum_{i=1}^{i=N} g(\tau_i, \gamma_i) \ , \tag{3.4}$$

where N is the number of depth points.

Starting at $\gamma(z) = 1$, we change the initial model such that Γ is maximized. To calculate this change in the interval-slowness model, we need to calculate the gradient of the objective function. The j-th component of the gradient of the objective function at the current model position, $\tilde{\mathbf{w}}$, is

$$\left.\frac{\partial \Gamma}{\partial w_j}\right|_{\mathbf{w}=\tilde{\mathbf{w}}} = \sum_{i=1}^{i=N} \left.\frac{\partial \Gamma}{\partial \gamma_i}\right|_{\mathbf{w}=\tilde{\mathbf{w}}} \left.\frac{\partial \gamma_i}{\partial w_j}\right|_{\mathbf{w}=\tilde{\mathbf{w}}} \ . \tag{3.5}$$

The derivative $\partial\Gamma/\partial\gamma_i$ can be calculated by finite differencing at each depth. The derivative

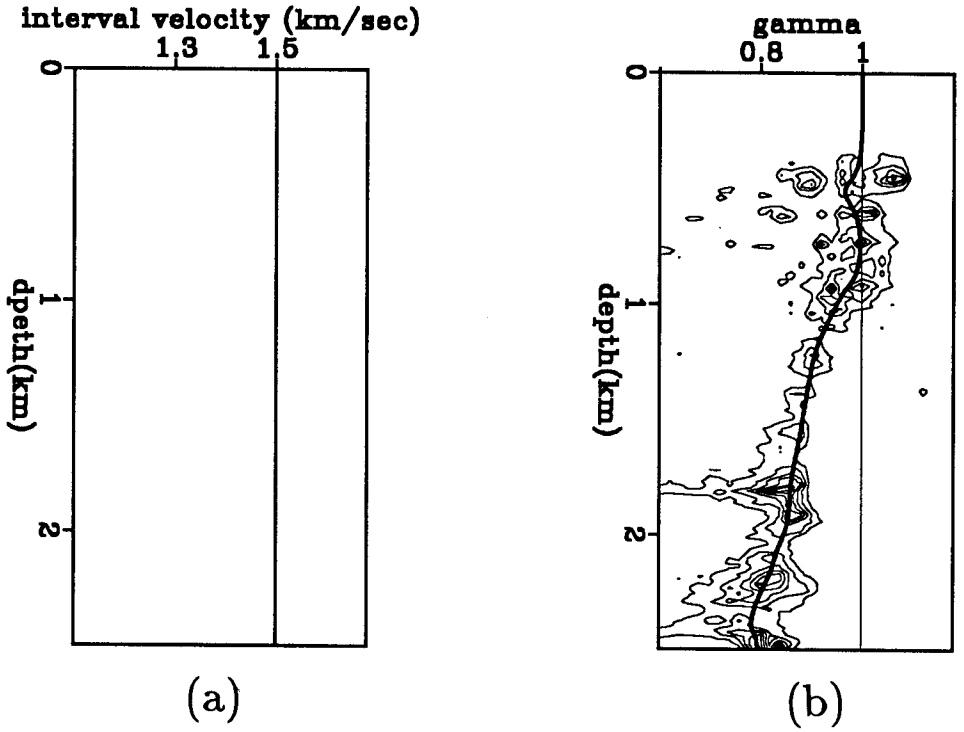

FIG. 3.1. (a) Interval-velocity model. The velocity in this model is constant. (b) Residual velocity panel. The light line is the position to which we want to drive the model. Once the model reaches this position, the velocity used in migration is the same as the velocity of the medium.

$\partial\gamma_i/\partial w_j$ is obtained analytically from the definition of γ in equation (2.4),

$$\begin{aligned} \gamma_i &= \frac{\bar{w}_i}{(\bar{w}_m)_i} \\ &= \frac{\frac{1}{i}\sum_{j=1}^{j=i} w_j}{\frac{1}{i}\sum_{j=1}^{j=i}(w_m)_j} . \end{aligned}$$

Therefore,

$$\begin{aligned} \frac{\partial\gamma_i}{\partial w_j} &= \frac{1}{\sum_{j=1}^{j=i}(w_m)_j} \qquad \text{for} \quad i \geq j , \\ &= 0 \qquad\qquad\qquad\quad \text{for} \quad i < j . \end{aligned}$$

A more straightforward method of obtaining interval slownesses is to start by assuming that the peaks in the residual velocity panel represent the error in the average slownesses. We then make a least-squares fit to these peaks thereby obtaining the average velocities. With these average slownesses we associate an interval-slowness model. To ensure that these average slownesses give reasonable interval slownesses, constraints are imposed on the interval-slowness model. These constraints may include smoothness (especially in the lateral direction) and any available a priori information about the velocity. It is well known that sharp variations in velocities cannot be detected by integral methods, namely methods that use only traveltime information (Stolt, 1986). If these sharp variations exist, they will show up in the reflectivity image obtained by migration. Also, unnecessary velocity variations in the lateral direction create imaginary fault-plane reflections (Clærbout, 1985). It is therefore sensible to impose a smooth-velocity-model requirement.

Let $\mathbf{w}'$ be the average slowness vector implied by the picked γ's, (using equation (3.3)); let $\hat{\mathbf{w}}$ be an a priory slowness model vector used as a constraint (if available); then we want to find $\mathbf{w}$ that minimizes

$$E = \sum_{j=1}^{j=N} \left[\bar{w}_j(w_i) - \bar{w}'_j\right]^2 + \alpha \sum_{i=1}^{i=N} \left[(w_i - w_{i-1})^2 + (w_i - w_{i+1})^2\right] + \beta \sum_{i=1}^{i=N} (w_i - \hat{w}_i)^2 \ , \quad (3.6)$$

where N is the number of layers, α and β are weights for the constraints, and bars denote averaging. The first summation in equation (3.6), minimizes the difference between the resulting average-slowness model, $\mathbf{w}$, and the picked average-slowness model, $\mathbf{w}'$. The second summation is the smoothing constraint; the difference between w_i and its neighbors w_{i-1} and w_{i+1} is minimized. The third summation minimizes the difference between the solution $\mathbf{w}$ and the a priori model $\hat{\mathbf{w}}$. The weights α and β penalize the model for going far from the constraints. Putting the weights outside the summation assumes that they are constant for all parts of the model. This assumption can be relaxed without change in the algorithm. Note that the interval slownesses are used implicitly in the first summation; they enter the summation via the average slownesses. However, the constraints in the other summations explicitly use interval slownesses.

To minimize E in equation (3.6), we take its derivative with respect to each w_i and

equate it to zero. Thus,

$$\sum_{j=1}^{j=N} \left[\bar{w}_j(w_i) - \bar{w}'_j\right] \frac{\partial \bar{w}_j}{\partial w_i} + \alpha\,(2w_i - w_{i-1} - w_{i+1}) + \beta(w_i - \hat{w}_i) = 0\ . \qquad (3.7)$$

Note that

$$\begin{aligned} \frac{\partial \bar{w}_j}{\partial w_i} &= \frac{1}{j} \qquad \text{for} \quad j \geq i \\ &= 0 \qquad \text{for} \quad j < i\ . \end{aligned}$$

Finding interval slownesses, therefore, amounts to solving the equation

$$\mathbf{A}\mathbf{w} + \mathbf{Tri}(-\alpha, 2\alpha+\beta, -\alpha)\mathbf{w} = \mathbf{B}\,\bar{\mathbf{w}}' + \beta\,\hat{\mathbf{w}}\ , \qquad (3.8)$$

where $\mathbf{A}$ is a matrix whose entries are

$$A_{ij} = \sum_{k=\max(i,j)}^{k=N} \frac{1}{k^2}\ ,$$

$\mathbf{B}$ is an upper triangular matrix whose entries are

$$\begin{aligned} B_{ij} &= \frac{1}{j} \qquad \text{for} \quad j \geq i \\ &= 0 \qquad \text{for} \quad j < i\ , \end{aligned}$$

and $\mathbf{Tri}(-\alpha, 2\alpha+\beta, -\alpha)$ is a tridiagonal matrix with $2\alpha+\beta$ as the diagonal elements and $-\alpha$ as the off-diagonal elements.

3.3 THE TWO-DIMENSIONAL PROBLEM

The analysis in the previous section treated each CRG independently. This treatment does not take into account lateral variations in velocity. When lateral velocity variations exist, all CRG's should be analyzed simultaneously.

In order to analyze CRG's simultaneously, the medium is divided into rectangular cells. The velocity errors in a CRG are then projected along all the ray paths and equation (3.8) is solved for each path. The corrections from all rays crossing a cell is averaged. This

projection of velocity error is similar to projection of traveltime error in tomographic techniques (e.g. Dines and Lytle, (1979))

3.4 RE-MIGRATING THE DATA

The velocity analysis method presented in this thesis involves re-migrating the data every time the velocity model is modified. Therefore, it is natural to ask whether we need to migrate the data from scratch every time or if we can do a *residual* prestack migration. In post-stack migration, the idea of residual migration is helpful, making expensive accurate migration possible by doing a number of cheap approximate steps (Rothman et al., 1985). It is natural to wonder if there is a parallel concept in prestack migration.

As mentioned in Chapter 1, for a constant velocity, prestack migration can be done by zero-offset (or post-stack) migration after NMO and DMO. If the data is migrated with a velocity v_1, the process is written as

$$image_1 = \mathbf{Mig_1}\ \mathbf{DMO_1}\ \mathbf{NMO_1}\ data\ , \tag{3.9}$$

where **NMO**, **DMO**, and **Mig** are the NMO, DMO, and post-stack migration operators. If the new velocity is v_2, then

$$image_2 = \mathbf{Mig_2}\ \mathbf{DMO_2}\ \mathbf{NMO_2}\ data\ . \tag{3.10}$$

We want to find the operator, **A**, that can be used to produce the new migrated image, $image_2$, from the previously migrated image, $image_1$. That is,

$$image_2 = \mathbf{A}\ image_1\ . \tag{3.11}$$

From equation (3.9), we have

$$data = \mathbf{NMO_1^{-1}}\ \mathbf{DMO_1}^{-1}\ \mathbf{Mig_1^{-1}}\ image_1\ . \tag{3.12}$$

Now, equation (3.10) becomes

$$\begin{aligned} image_2 &= \mathbf{Mig_2\ DMO_2\ NMO_2\ NMO_1^{-1} DMO_1^{-1}\ Mig_1^{-1}}\ \ image_1 \\ &= \mathbf{Mig_2\ DMO_2\ NMO_{12}\ DMO_1^{-1}\ Mig_1^{-1}}\ \ image_1\ , \end{aligned} \tag{3.13}$$

where $\mathbf{NMO_{12}}$=$\mathbf{NMO_2\ NMO_1^{-1}}$ is the residual NMO operator. If s_1 is the slowness used in the first NMO and s_2 is the slowness used in the second NMO, the residual NMO is done by NMO with a slowness $s = \sqrt{s_2^2 - s_1^2}$ if $s_2 > s_1$, or inverse NMO with a slowness $s = \sqrt{s_1^2 - s_2^2}$ if $s_1 > s_2$. Therefore, we have found the operator $\mathbf{A}$ to be

$$\mathbf{A = Mig_2\ DMO_2\ NMO_{12}\ DMO_1^{-1}\ Mig_1^{-1}}\ . \tag{3.14}$$

Nothing can be done to simplify the operator $\mathbf{A}$ because the NMO, DMO, and migration operators do not commute. Because $\mathbf{A}$ is not a prestack migration operator, re-migrating the migrated profiles cannot be done by another prestack migration operator.

This conclusion implies that we need to re-migrate the data from scratch every time we modify the velocity model. The reason for this conclusion is the non-commutativity of the operators. In Al-Yahya and Fowler (1986), we arrive at the same conclusion by this and other considerations. The most interesting of those considerations is the nonlinearity of the double-square-root equation which is used in prestack migration.

3.5 A FIELD DATA EXAMPLE

The input to the velocity analysis scheme presented here is field profiles. In this example I used marine profiles from the Gulf of Mexico. These profiles are well-sampled in the receiver axis (receiver spacing is 12.5 m), and have been sub-sampled in the shot axis (to make the source spacing 50 m). This arrangement is most suitable for profile processing in which the receiver axis is the critical one and it need to be well-sampled while the shot axis need not be heavily sampled. Two profiles are shown in Figure 3.2 and 3.3; a total of 28 profiles were used, each having 240 receivers. Note the fault-plane reflection that appears in both profiles.

The first step in the velocity analysis method of this thesis is migrating all profiles with a preliminary velocity model. A model obtained by a rough conventional velocity analysis

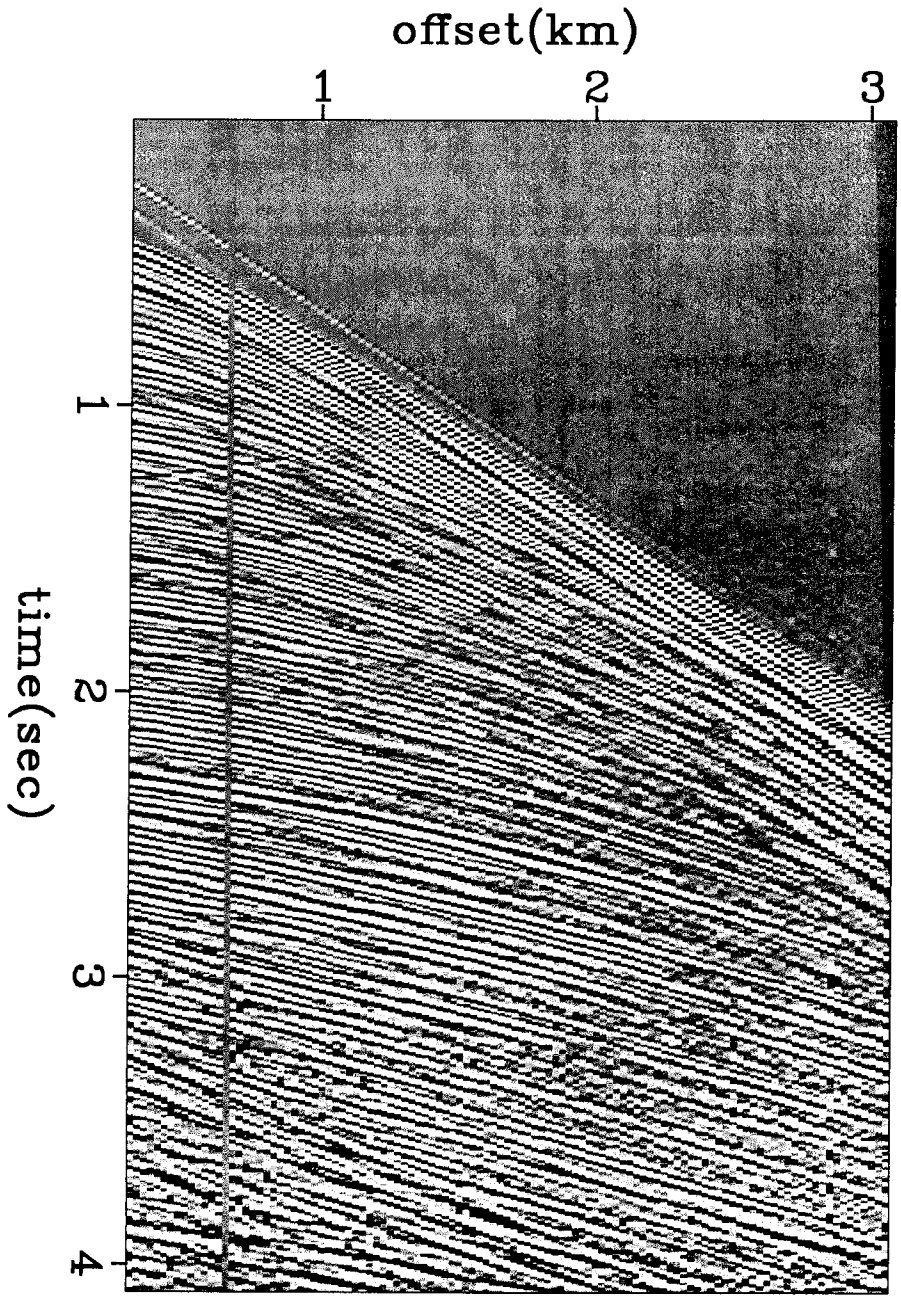

FIG. 3.2. A typical marine profile used for velocity analysis example. Note the fault-plane reflection at about 1.3 sec.

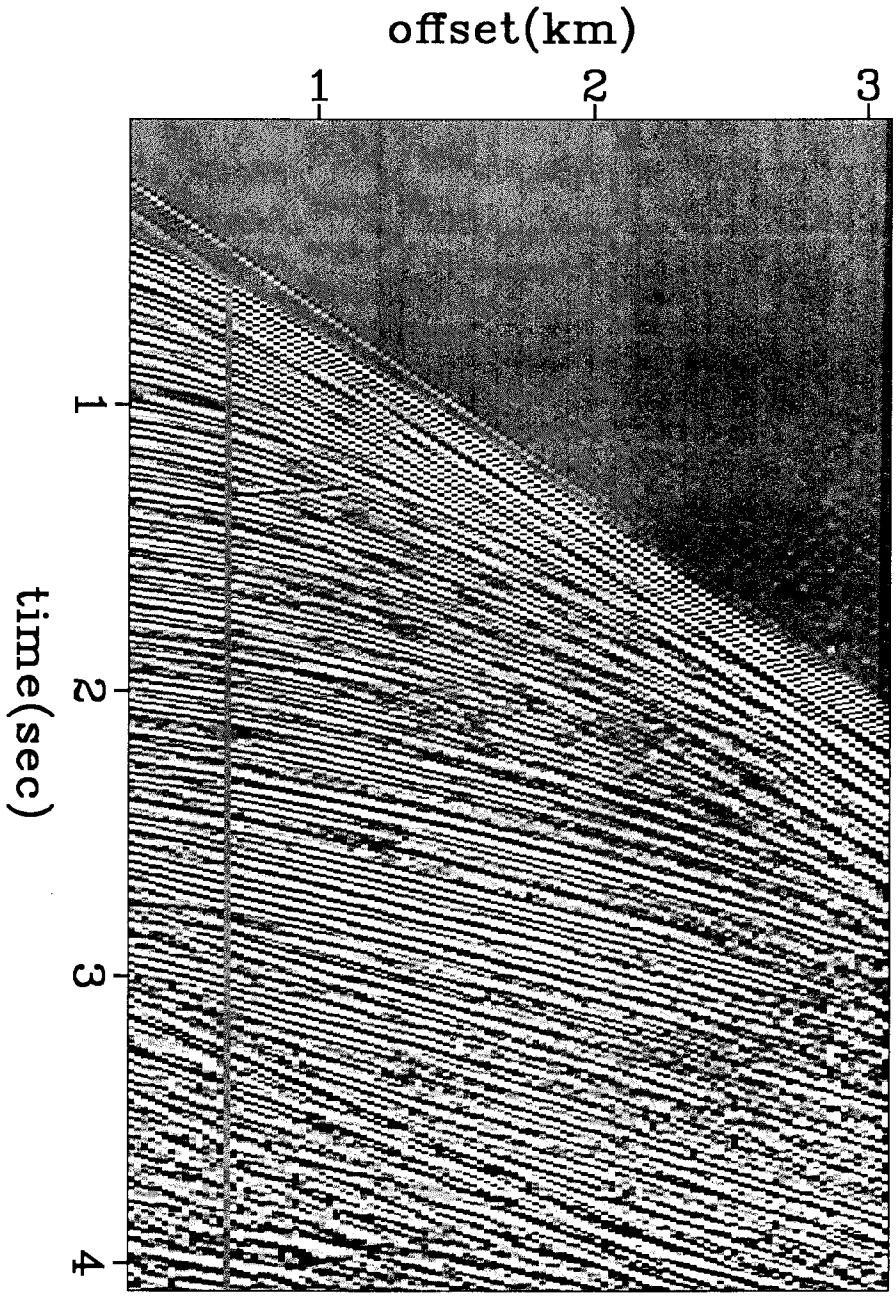

FIG. 3.3. Another marine profile from the survey. Note that the same fault-plane reflection that appears in Figure 3.2 appears here, but at different offsets.

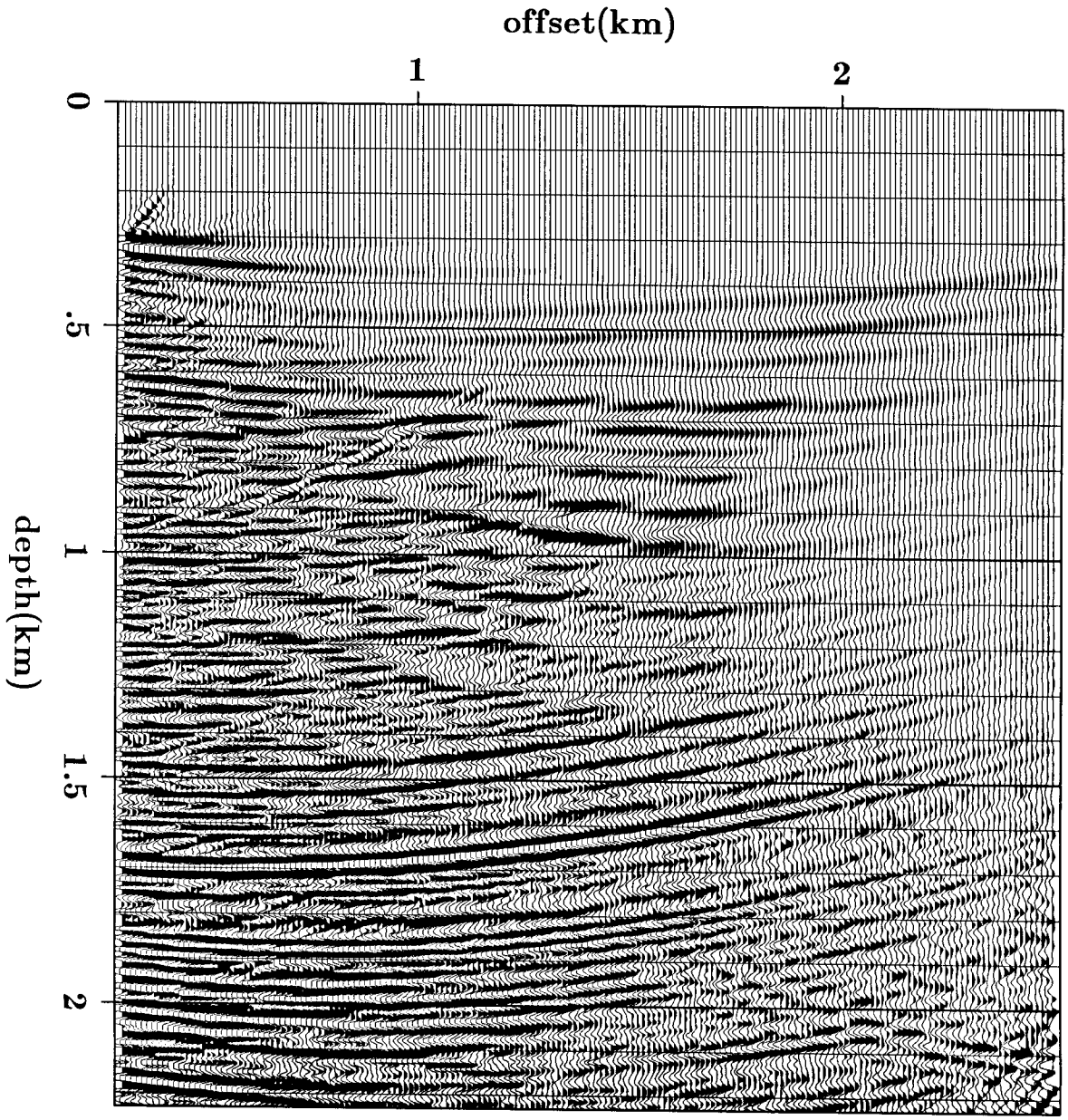

FIG. 3.4. The profile of Figure 3.2 after migration with water velocity. Note the edge diffractions. These diffractions are attenuated after stacking (see Figure 3.5).

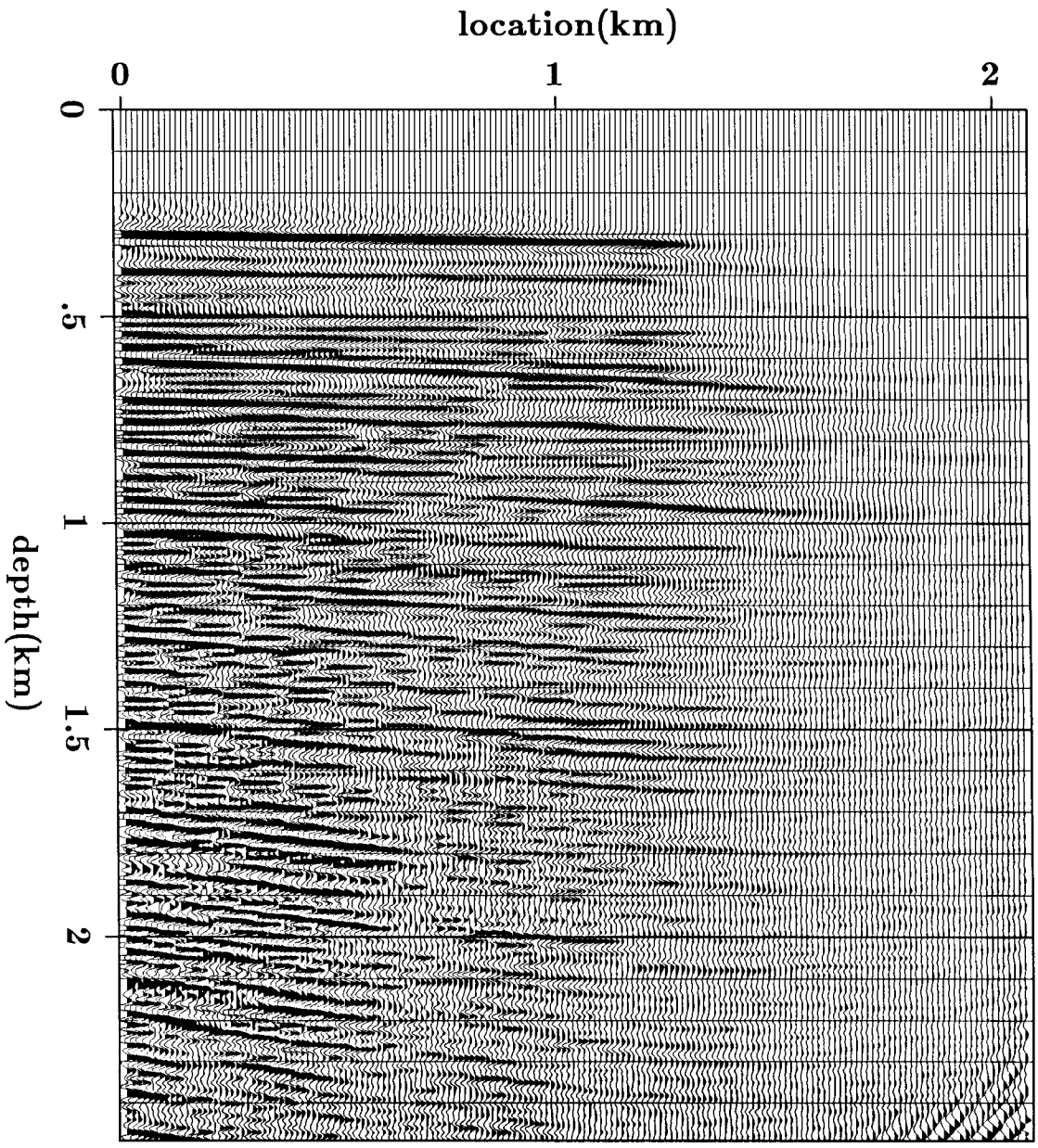

FIG. 3.5. The image obtained by migrating and stacking the profiles with the water velocity. Note that the fault-plane reflection between .5 and 1 km is somewhat coherent, indicating that the error in velocity at that depth is small. Also note that the edge diffractions which appeared in Figure 3.4 have been attenuated by stacking.

can serve as a preliminary model. In this example, I used a constant-velocity model that has the velocity of water (1.5 km/sec). Figure 3.4 shows the result of migrating the profile in Figure 3.2 with this velocity and Figure 3.5 shows the stacked section, obtained by summing along the shot axis. Only the water bottom is imaged correctly because the velocity used in migration was correct only down to the water bottom. Below the water bottom, the migrated profiles and stacked section do not represent the geology correctly. Note the diffractions in Figure 3.4 which are caused by the finite cable length and some boundary reflections (even though absorbing boundaries were used). These diffractions are attenuated after stacking (as in Figure 3.5) if overlapping of profiles is dense enough; overlapping of ten or fifteen profiles is considered dense enough. Note that the fault-plane reflection is somewhat coherent indicating that the error in velocity at that depth is small.

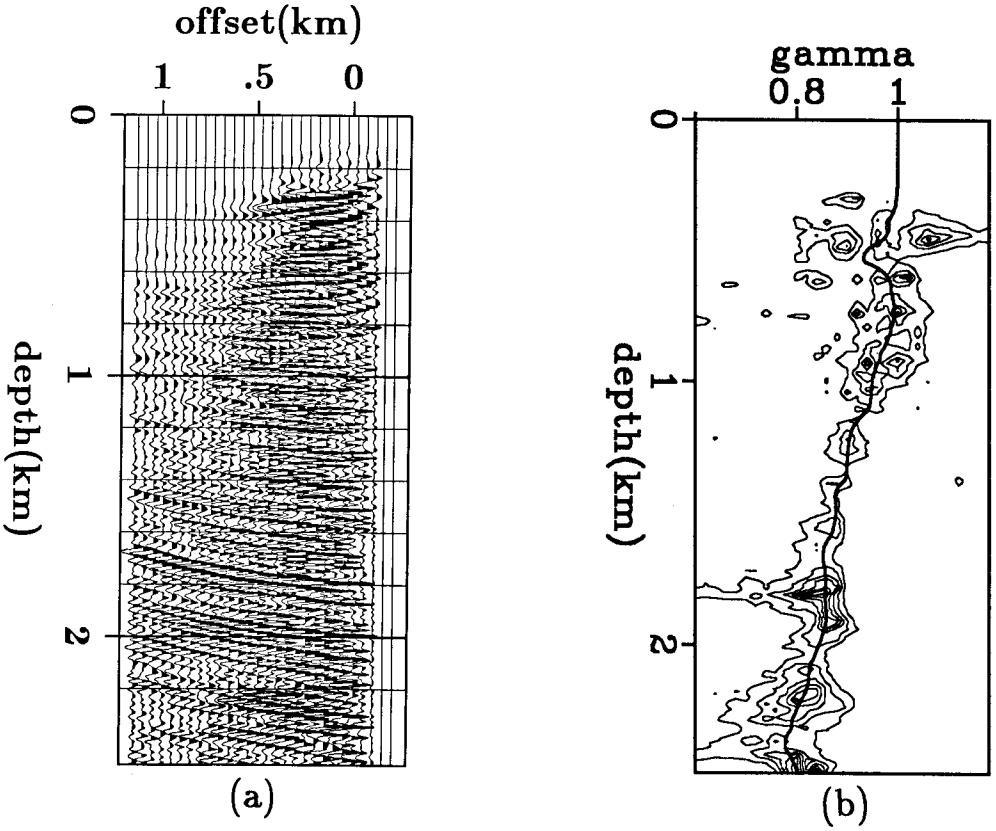

FIG. 3.6. (a) A typical post-migration CRG obtained from profiles migrated with the water velocity. (b) A semblance panel obtained from the CRG in (a). The heavy line through the peaks gives the slowness ratio γ vs. depth. This curve is used to compute average slownesses. No constraints on interval velocities are imposed at this stage. They are imposed later when computing interval velocities.

The next step is to sort the data to produce common-receiver gathers (CRG's) from the migrated profiles. A typical CRG is shown in Figure 3.6a. Note that only the water bottom (at about .35 km) is flat. Other events are curved upward indicating that the velocity that was used in migration was lower than the velocity of the medium for those depths. By searching for curvature as a function of depth, the panel shown in Figure 3.6b is produced. From this panel we obtain average slownesses from which interval slownesses (or velocities) need to be computed. Note that the curve through the peaks is made reasonably smooth but it is not constrained to give reasonable interval velocities. The constraints are introduced later when interval velocities are computed.

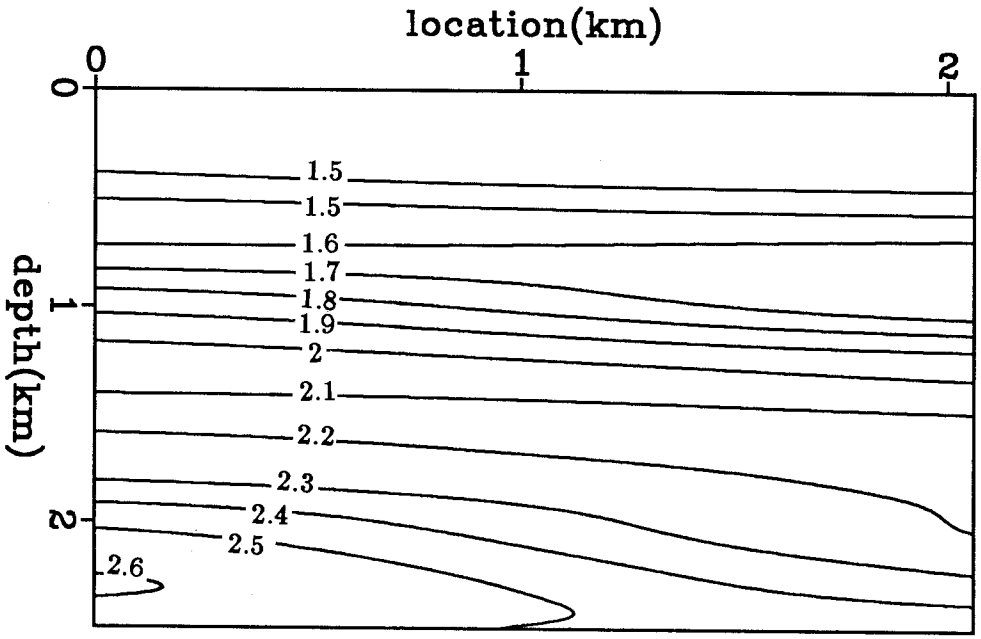

FIG. 3.7. A contour plot of the interval-velocity model obtained from the first iteration using the semblances in Figure 3.6. Contour labels are velocities in km/sec.

The method outlined in the previous sections was used to compute interval velocities and the result is the model shown in Figure 3.7. This model was obtained from one iteration and may therefore have errors, but it should be closer to the real velocity model than the constant-velocity model I used initially.

Figure 3.7 concludes the first iteration. We are ready to start the second iteration

using the new velocity model as the starting model. The above sequence is repeated for the second iteration. Figure 3.8 shows a profile migrated with this velocity model and Figure 3.9 shows the stacked section. Note that reflectors are now more continuous than they appear in Figure 3.5. The fault-plane reflection is also more coherent now.

To correct the error in the model of Figure 3.7, we examine the post-migration CRG's. A typical CRG is shown in Figure 3.10a, and the semblance panel is shown in Figure 3.10b. We see that when the new velocity model is used, most images are now close to the curve $\gamma = 1$ in the semblance panel meaning that the migration velocity is close to the velocity of the medium. Some deep images slightly curve upward, however (making $\gamma < 1$). The water bottom reflection is also slightly curved downward which means that the velocity used in migration above the water bottom is slightly higher than the water velocity.

The interval-velocity model obtained from analyzing the post-migration CRG's is shown in Figure 3.11. Figure 3.12 shows a profile migrated with the velocity model of Figure 3.11 and Figure 3.13 shows the stacked section. Most of the differences between Figure 3.9 and Figure 3.13 occur in the deep reflectors where they are more coherent in the latter.

We could go on and do more iterations. However, the CRG and the semblance panel shown in Figure 3.14 indicate that the velocity model we have reached is reasonably close to the true velocity model. Events in the CRG are now aligned horizontally satisfying the velocity analysis principle described in this thesis.

Chapter 2 mentions that the strength of the signal in the stacked section is a measure of the "goodness" of the velocity model and that we can search for a velocity model that has the strongest signal. From an optimization point of view, the strength of the signal is the objective function that we maximize as we search for the best velocity model. The strength of the signal can be measured by the power of the stack, defined as the sum of the squares of all points in the stack. Therefore, if we compute the power of the stack in the example that is discussed here, we expect to see it increase from one iteration to the next. This is the case in Figure 3.15 which shows the power of the stack as a function of iteration. Note that the power increases five-fold in two iterations and most of the increase is in the first iteration.

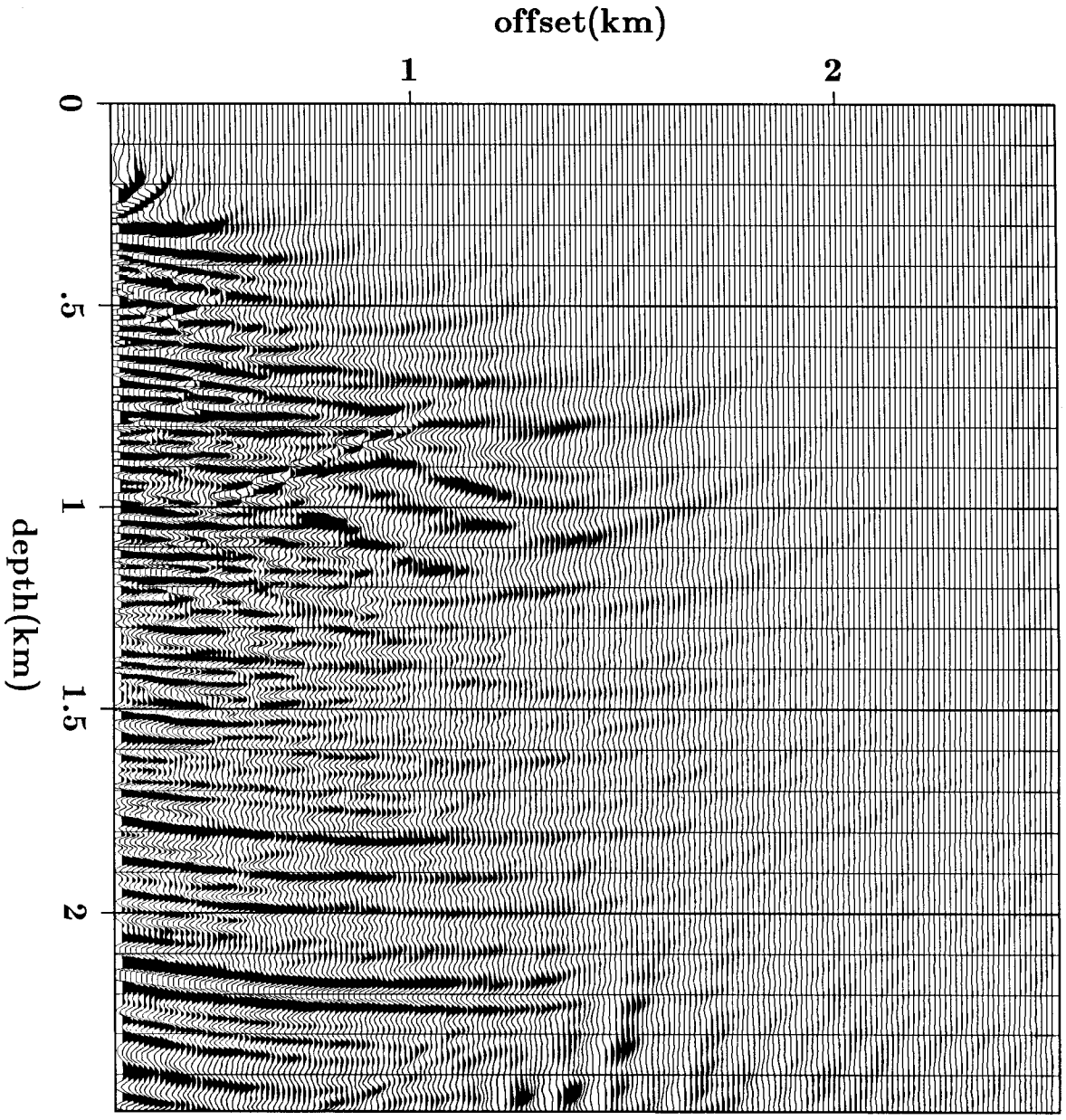

FIG. 3.8. The profile of Figure 3.2 after migration with the velocity model in Figure 3.7. Note the edge diffractions. These diffractions are attenuated after stacking (see Figure 3.9).

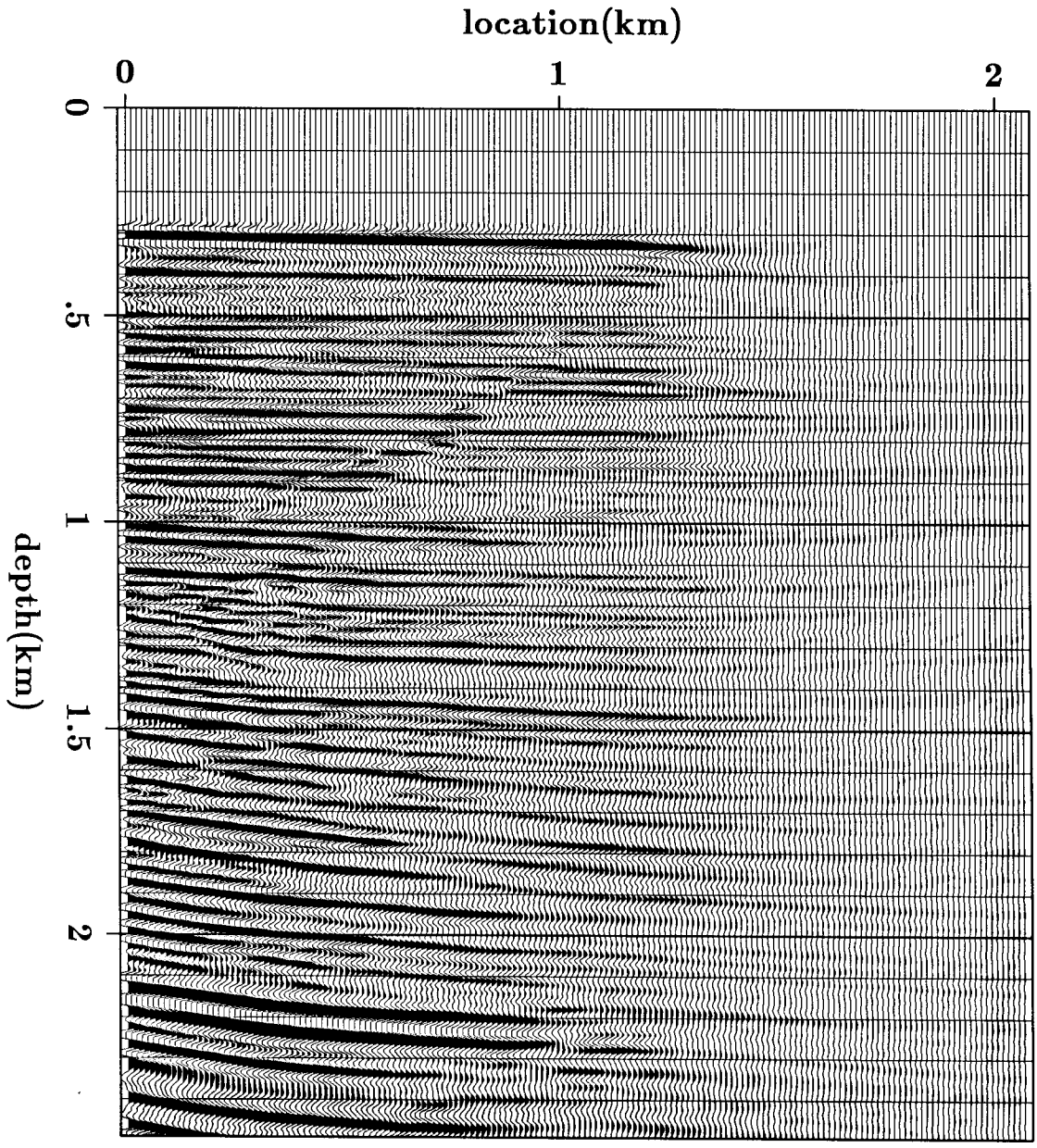

FIG. 3.9. The image obtained by migrating and stacking the profiles with the model in Figure 3.7. Compare it to the stack of Figure 3.5. Note the coherency of the fault-plane reflection between .5 and 1 km. Also note that the edge diffractions which appeared in Figure 3.8 have been attenuated by stacking.

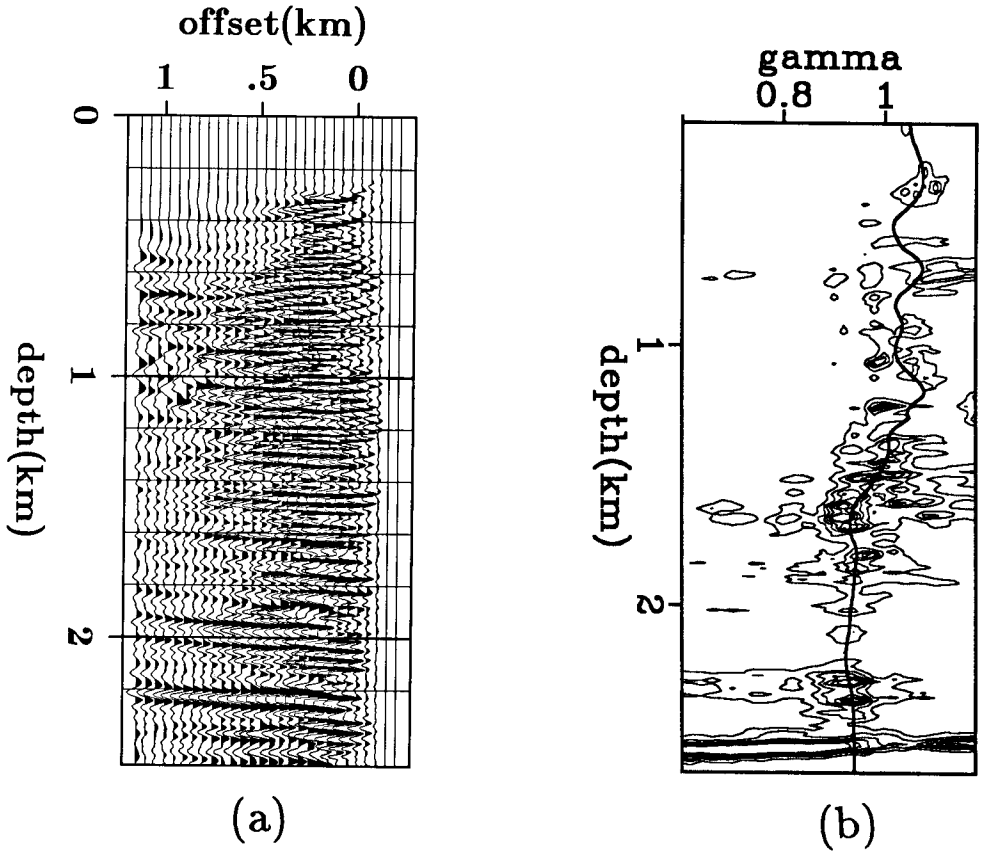

FIG. 3.10. (a) A typical post-migration CRG obtained from profiles migrated with the velocity model in Figure 3.7. (b) A semblance panel obtained from the CRG in (a). The heavy line through the peaks gives the slowness ratio γ vs. depth.

3.5.1 Comparison with conventional processing

I applied conventional processing to the same data set that was analyzed in the previous section. Velocity analysis was done by hand-picking from conventional velocity panels. The data was NMO-ed using these velocities and then it was stacked and migrated. The interval-velocity model that was used in the post-stack migration was obtained from stacking velocities by the Dix equation.

Figure 3.16 shows this interval-velocity model. This model is different from the model in Figure 3.11 which was obtained by the method described in this thesis. Note that the model in Figure 3.16 was obtained from picked rms velocities and that the model was not adjusted to fulfill any requirement. In contrast, the model in Figure 3.11 was based on the alignment of images and was adjusted iteratively to maximize this alignment. Note also

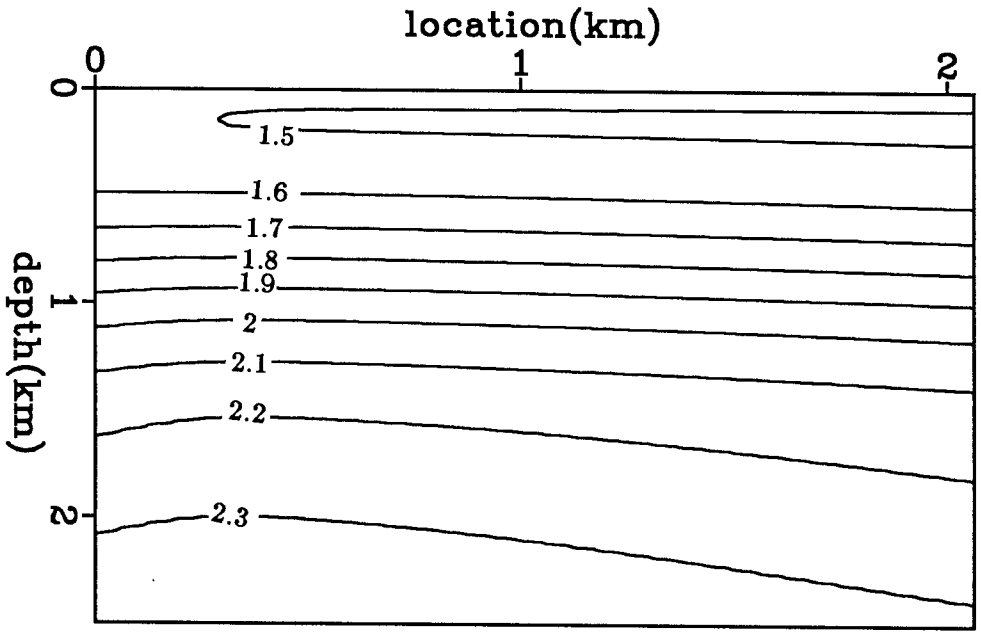

FIG. 3.11. A contour plot of the interval-velocity model obtained from the third iteration using the semblances in Figure 3.10. Contour labels are velocities in km/sec.

that the interval-velocity model shown in Figure 3.16 was obtained from rms velocities. As explained previously, obtaining interval velocities from rms velocities is very sensitive to errors.

Another way of comparing conventional velocity analysis with the method presented here is through the rms velocities, as shown in Figure 3.17. The figure shows that the rms velocities given by the two methods are different, especially near the bottom. In Figure 3.17a, the two velocities are not far apart and they follow the same trend. In Figure 3.17, however, the discrepancy between the two velocities is greater. This difference in velocities is expected to give different migrated images.

Figure 3.18 shows the migrated stacked section. Note that the fault-plane reflection which appears between .5 and 1 km in Figure 3.13 is absent in Figure 3.18. This absence of fault-plane reflection is expected because those reflections are attenuated by using stacking velocities that are too low for the fault-plane reflection. The differences between Figure 3.13 and 3.18 are mainly due to the difference in velocities used in processing the two images

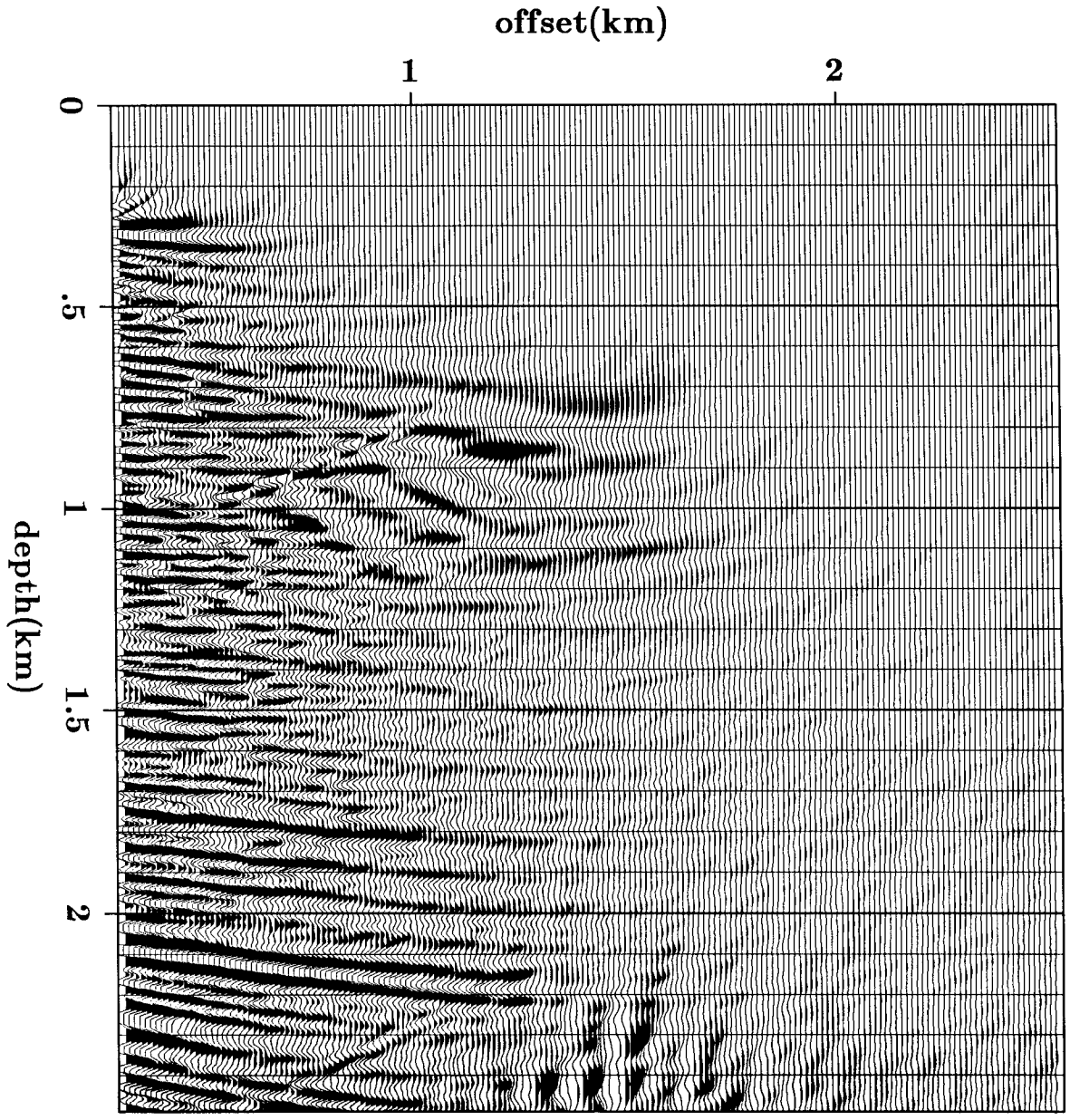

FIG. 3.12. The profile of Figure 3.2 after migration with the velocity model in Figure 3.11. Note the edge diffractions. These diffractions are attenuated after stacking (see Figure 3.13).

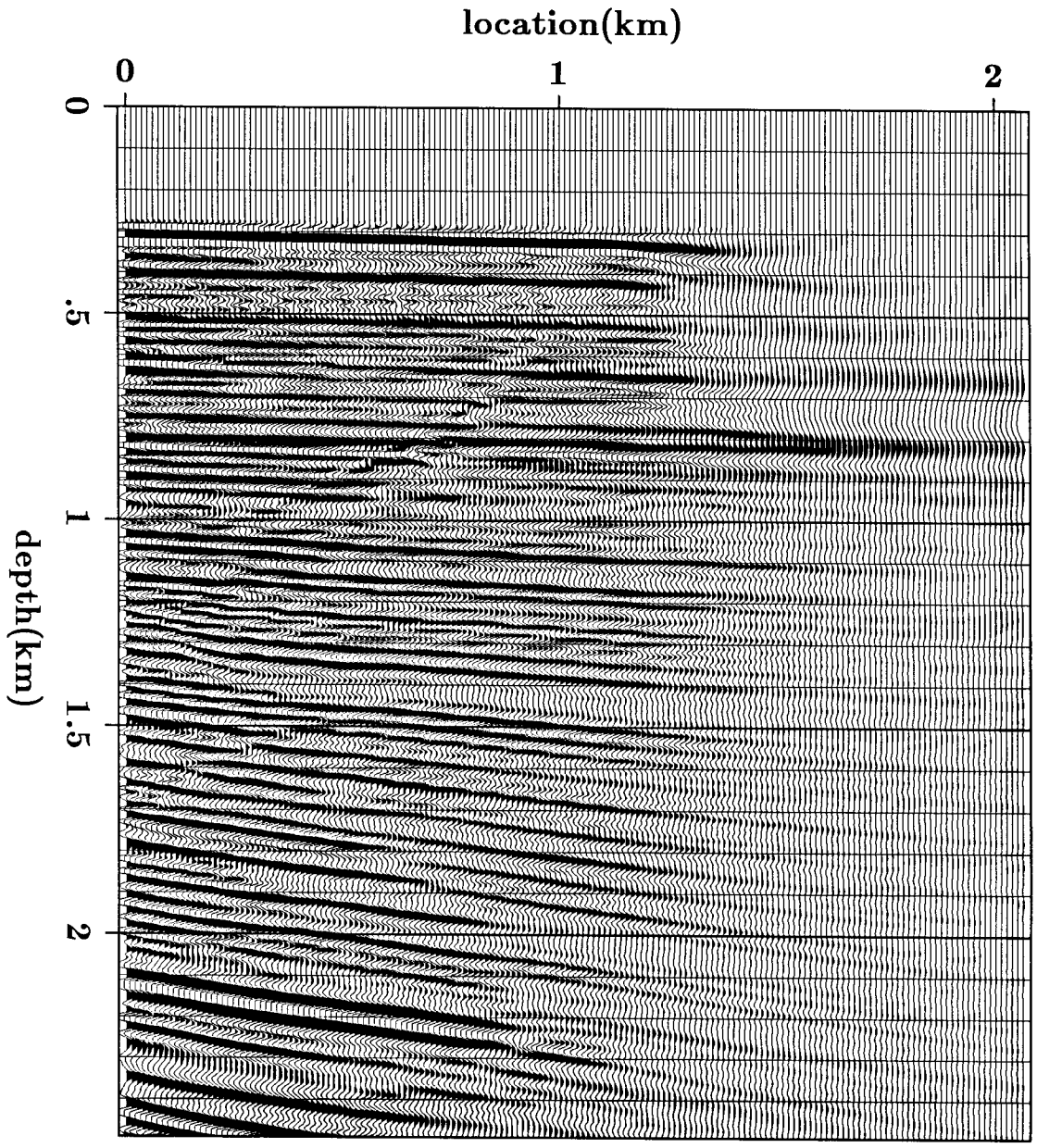

FIG. 3.13. The image obtained by migrating and stacking the profiles with the model in Figure 3.11. Compare the strong reflector at about 2.1 km with that in Figure 3.9. Also note that the edge diffractions which appeared in Figure 3.12 have been attenuated by stacking.

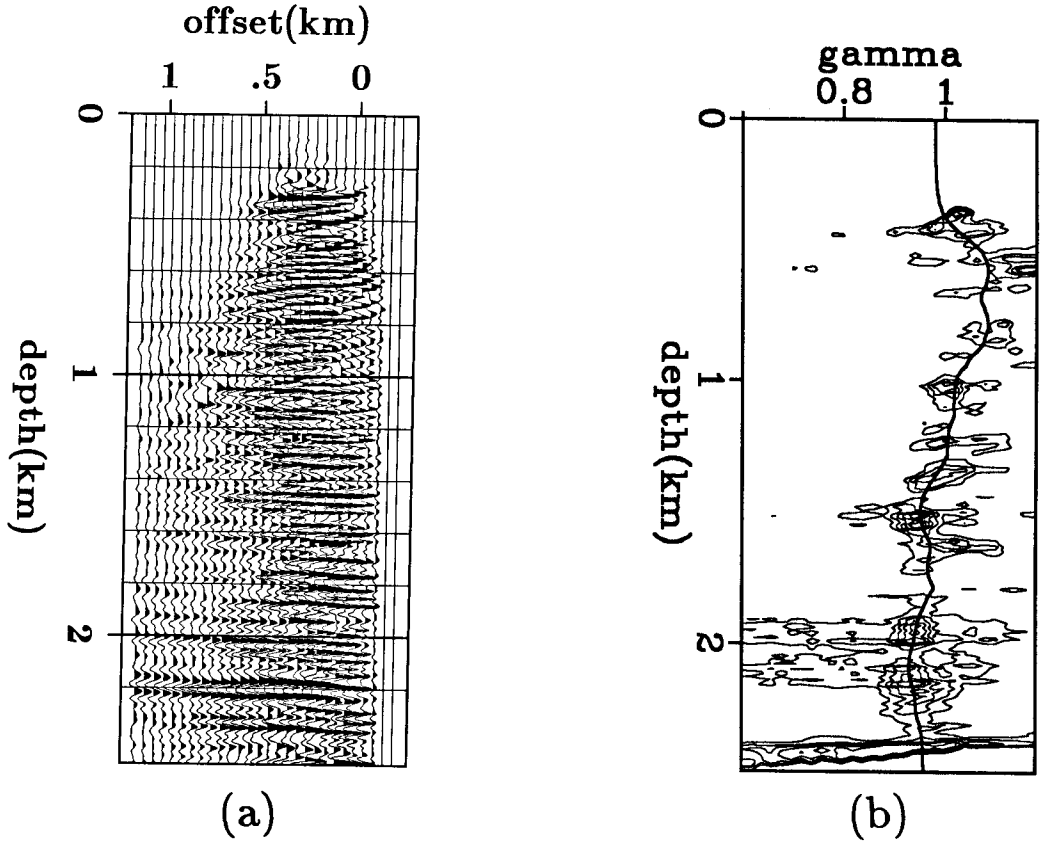

FIG. 3.14. (a) A typical post-migration CRG obtained from profiles migrated with the velocity model in Figure 3.11. (b) A semblance panel obtained from the CRG in (a). The heavy line through the peaks gives the slowness ratio γ vs. depth.

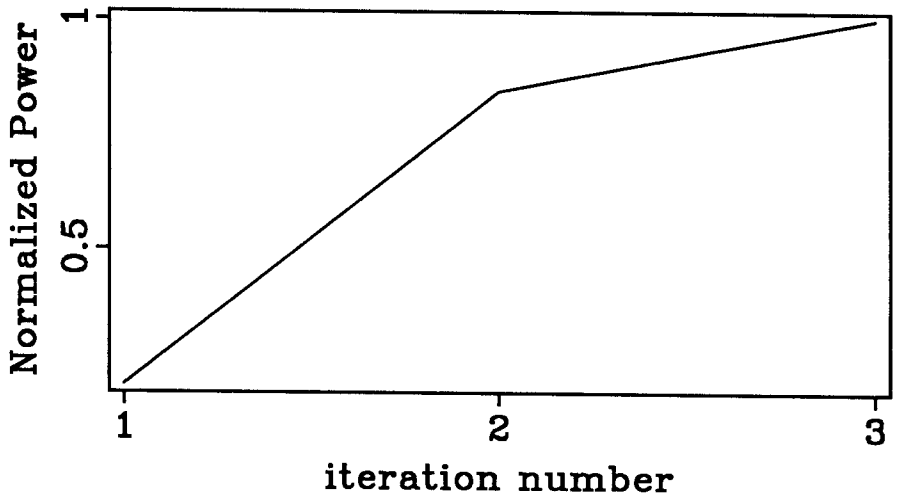

FIG. 3.15. Power of the stack as a function of iteration for the example discussed in this section. The first iteration is the starting model of constant velocity.

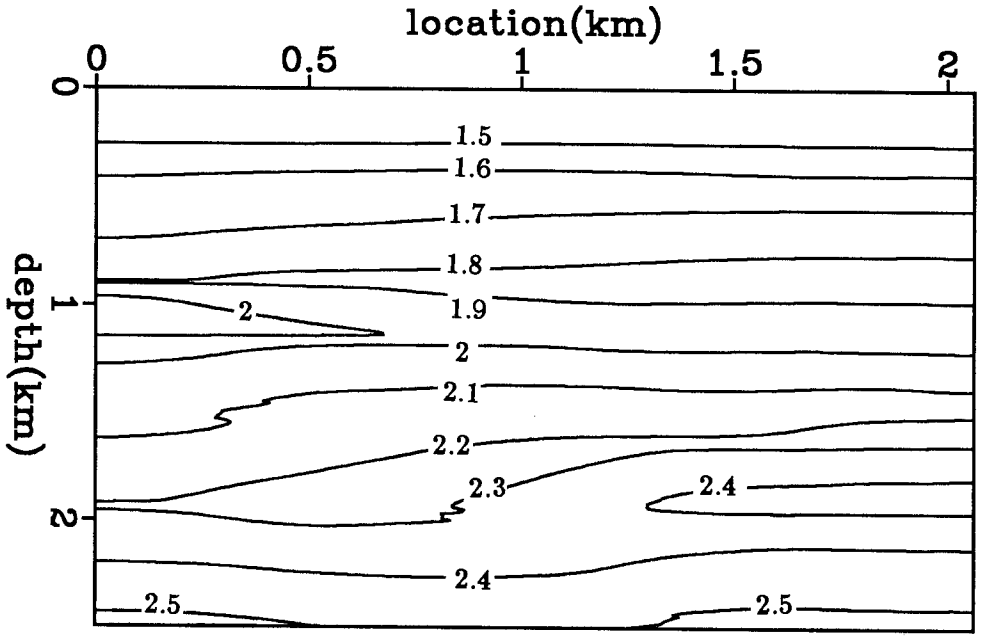

FIG. 3.16. Interval-velocity model obtained from conventional processing. Compare this figure to Figure 3.11.

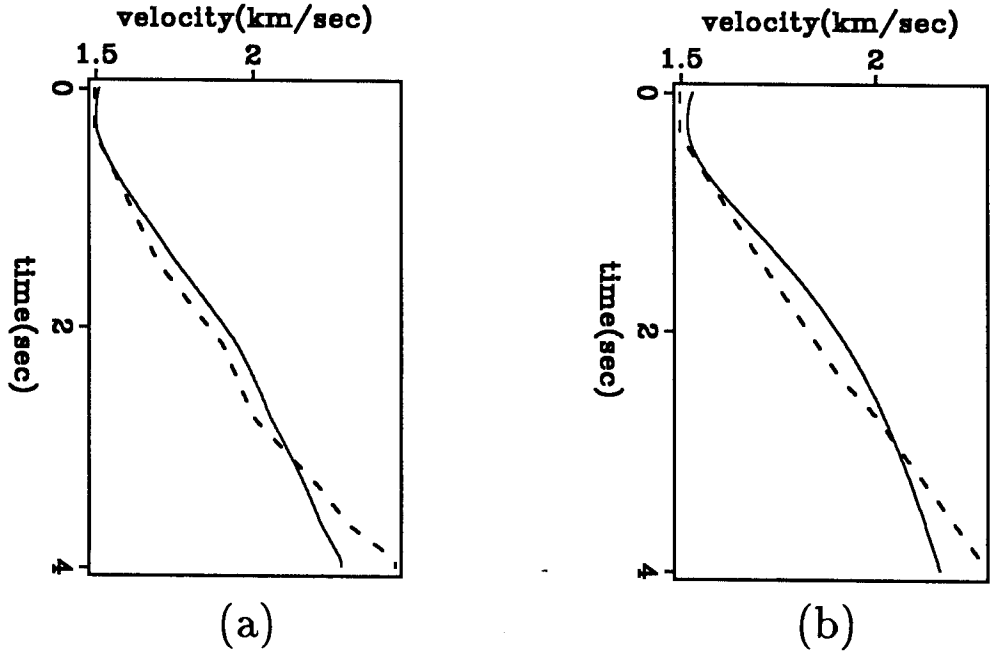

FIG. 3.17. Comparison of rms velocities at two locations. The solid curve is the curve obtained from the method presented here and the dashed curve is obtained from conventional processing. In both cases the two methods do not give identical results, especially in (b). At both locations, there is a large discrepancy near the bottom.

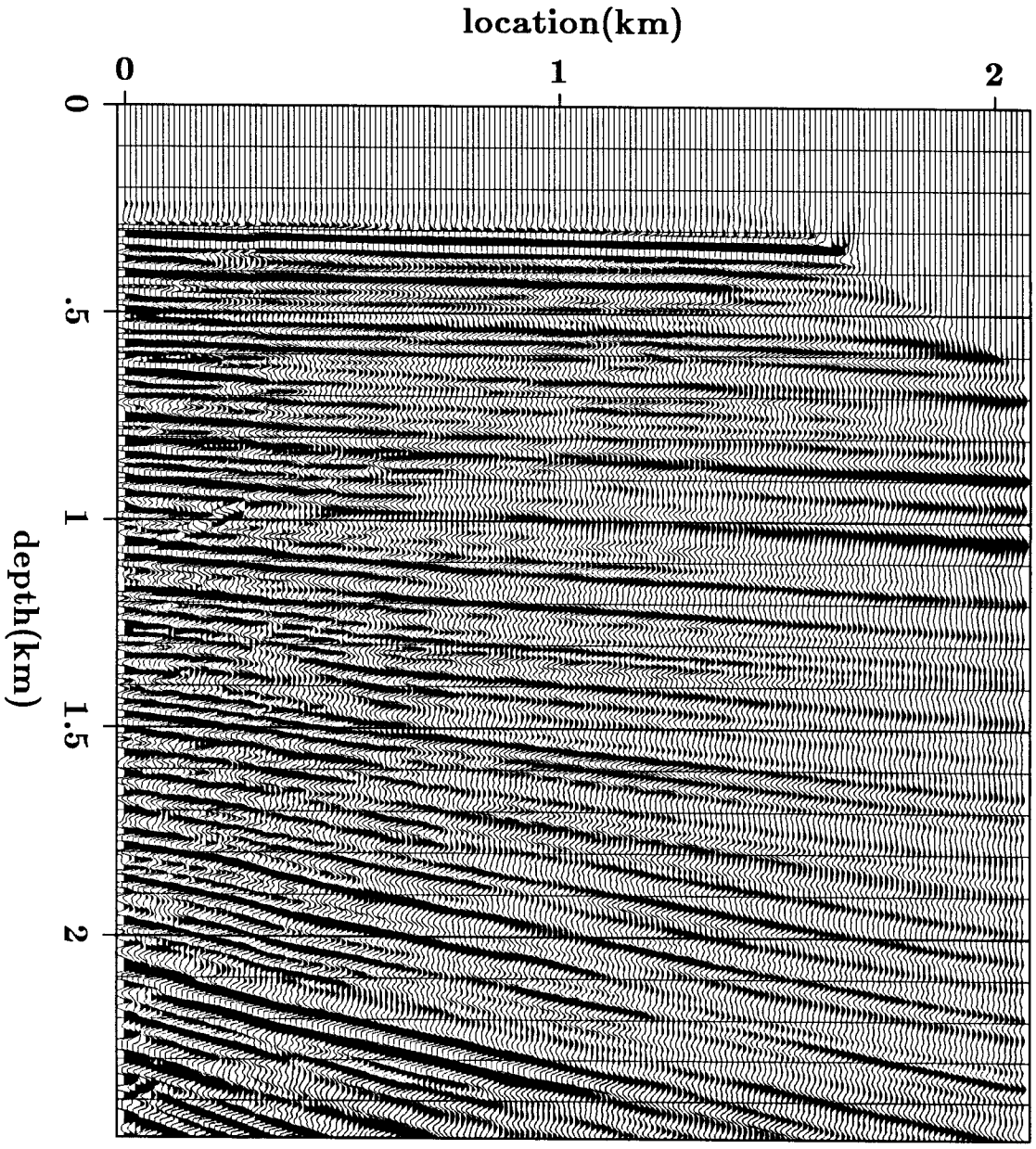

FIG. 3.18. The image obtained by conventional velocity analysis followed by NMO, stacking and migration. Compare this figure to Figure 3.13.

3.6 A SYNTHETIC EXAMPLE

The field data example described in the previous section did not have significant lateral velocity variations. To see how the method works when there is lateral velocity variation, a synthetic model is used in this section. The model, shown in Figure 3.19, has lateral velocity variation because of the anticlines and the wedge. It also has strong vertical velocity variations at some interfaces.

Like the field data example, the first preliminary model used in migrating the data has a constant velocity of 1.5 km/sec. Figure 3.20 shows the migrated and stacked section and Figure 3.21 shows a CRG and a semblance panel. Below the top reflector, velocity is too low. This is manifested in the CRG by the upward curvature of images. These curvatures are used to modify the initial model. The result is the model shown in Figure 3.22. Even though this model is not close to the true model yet, it is a better model than the constant-velocity model I initially used. It shows a high-velocity region between .5 and 1 km, followed by a lower velocity region, but it does not show the anticlines clearly. Note that at the left and right edges of the model, there is not enough coverage to provide information about the velocity. In Figure 3.22 and later figures, only those parts of the model that have enough coverage will be shown.

When the profiles are migrated with the model in Figure 3.22, the stacked section of Figure 3.23 is obtained. Figure 3.24 shows some post-migration CRG's in which the lowest two images still have some curvature. After four iterations, the velocity model in Figure 3.25 is obtained. Note that some artifacts exist in the final model that did not exist in the original model. These artifacts result from the lack of constraints between reflectors; the velocity can vary between two reflectors without affecting the image. The post-migration CRG's shown in Figure 3.26 have images which are aligned horizontally which means that the process has converged. The corresponding stacked section is shown in Figure 3.27. This stacked section shows the reflectivities in the model. Note that although the velocity model obtained by the velocity analysis was not identical to the original model, the reflectivity map, namely the migrated and stacked section, closely resembles the original model.

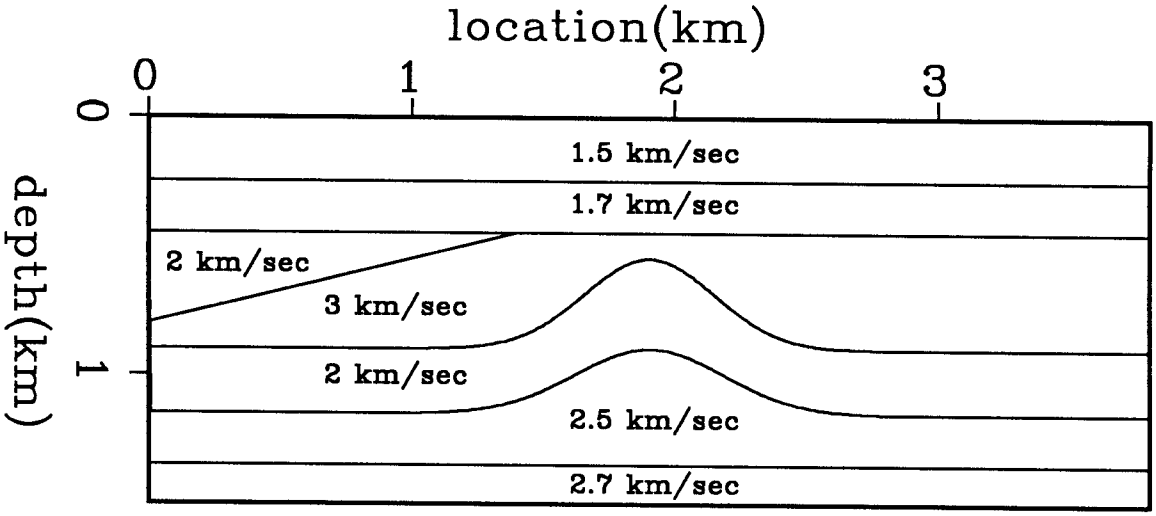

FIG. 3.19. The synthetic model which is used as an example.

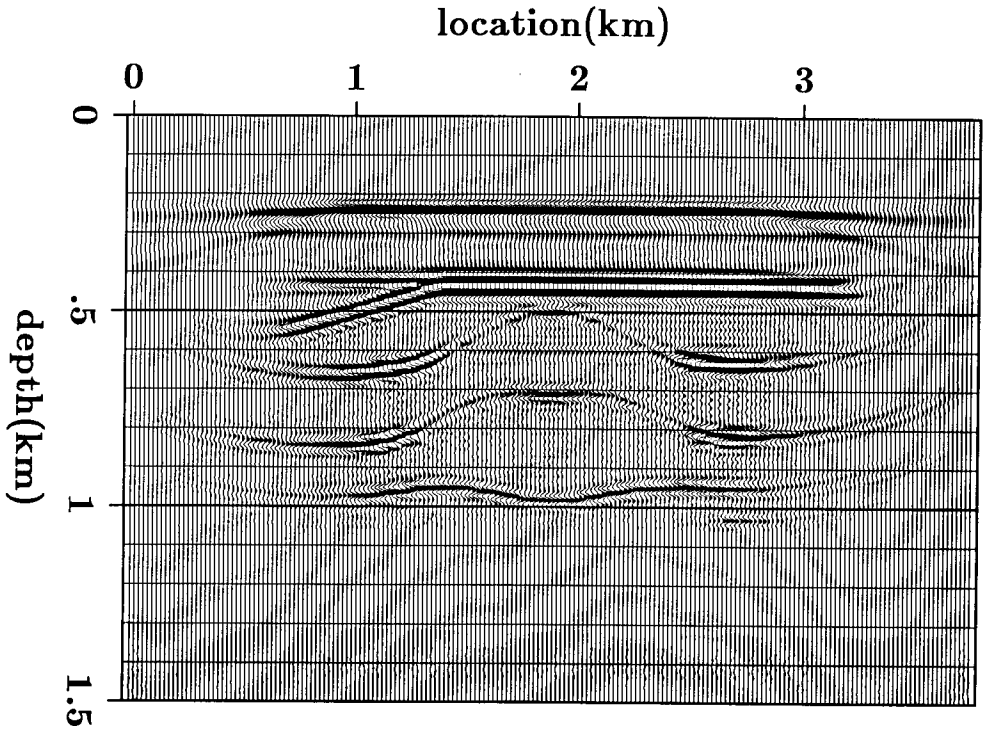

FIG. 3.20. The image obtained by migrating the synthetic profiles with a constant velocity of 1.5 km/sec and stacking.

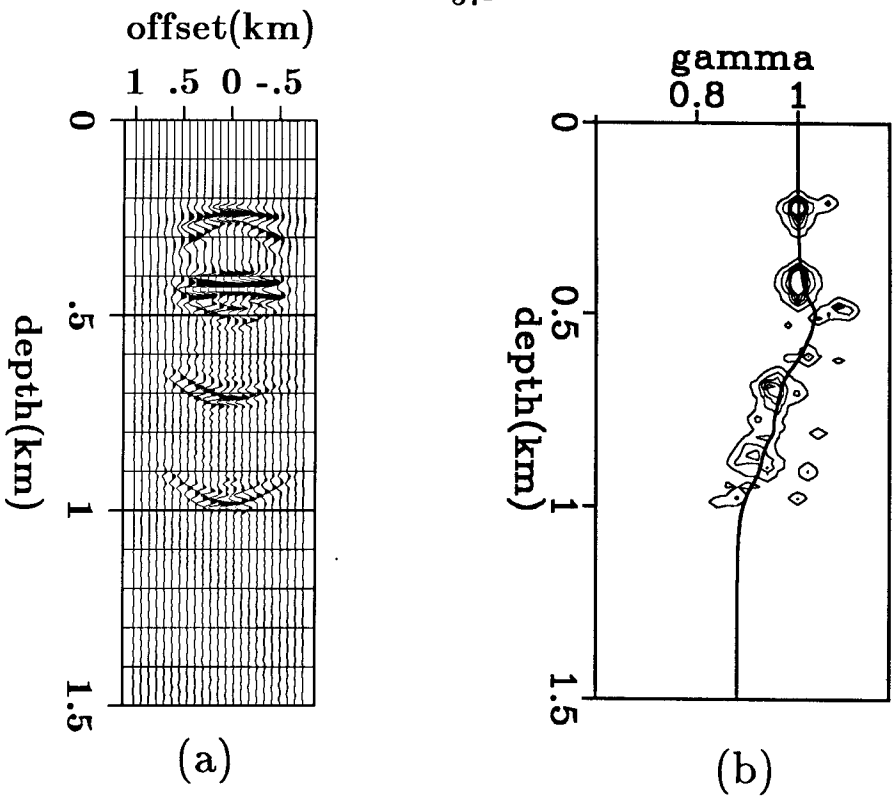

FIG. 3.21. (a) A post-migration CRG obtained from the synthetic profiles migrated with a constant velocity of 1.5 km/sec. (b) A semblance panel obtained from the CRG in (a). The heavy line through the peaks gives the slowness ratio γ vs. depth.

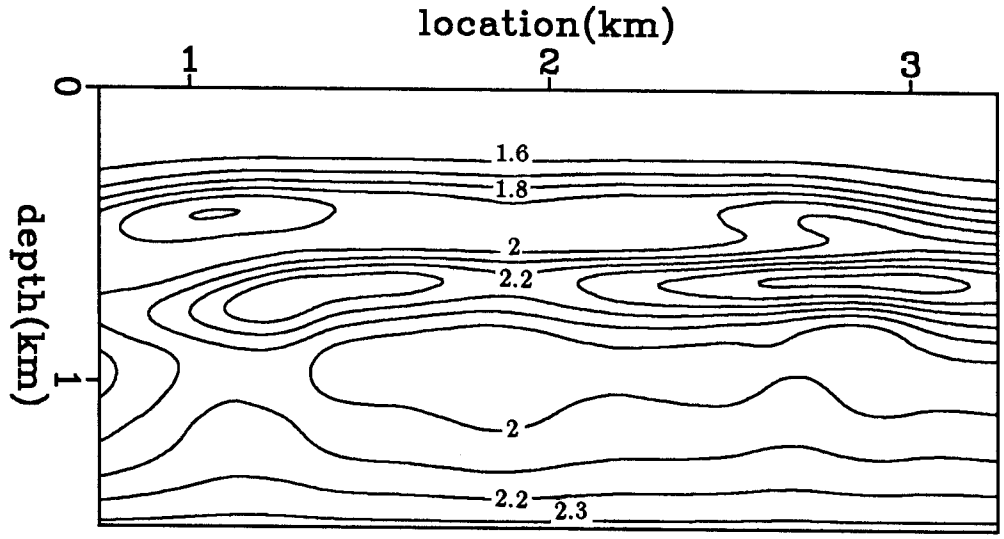

FIG. 3.22. A contour plot of the interval-velocity model obtained from the first iteration from the synthetic data using the semblances in Figure 3.21. Contour labels are velocities in km/sec.

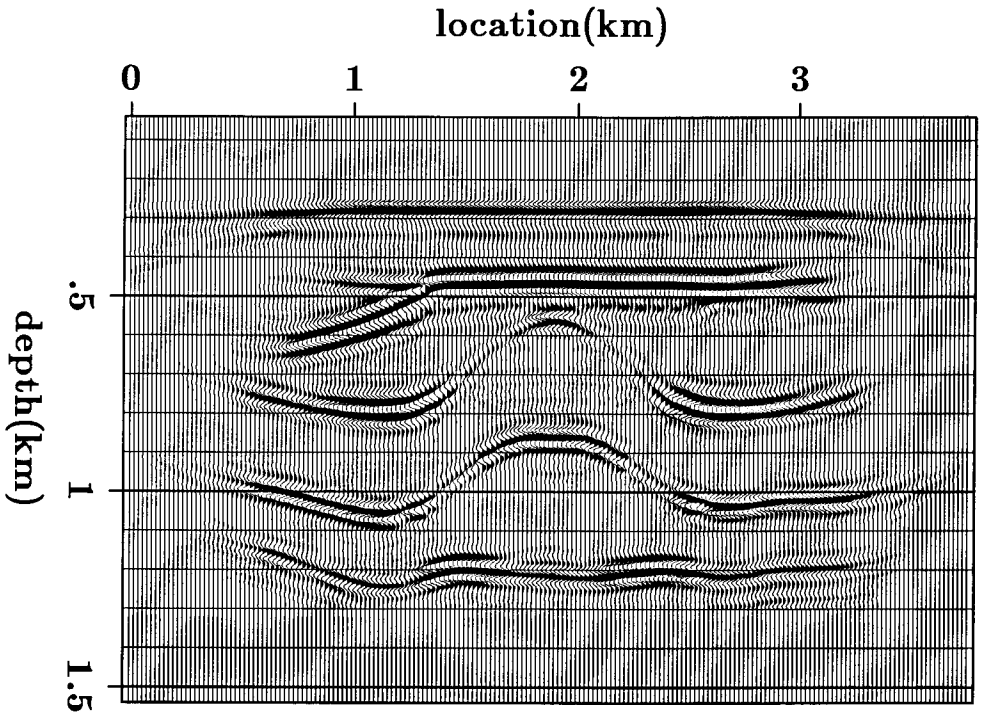

FIG. 3.23. The image obtained by migrating the synthetic profiles with the velocity model in Figure 3.22 and stacking.

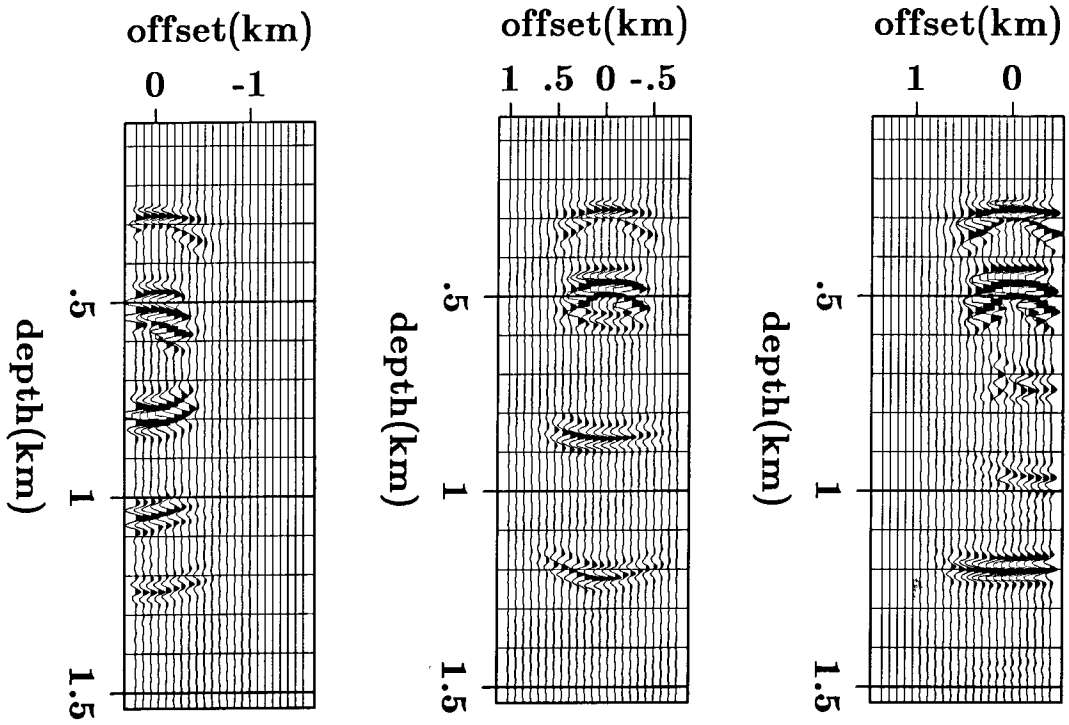

FIG. 3.24. Some post-migration CRG's obtained from the synthetic profiles migrated with the velocity model in Figure 3.22.

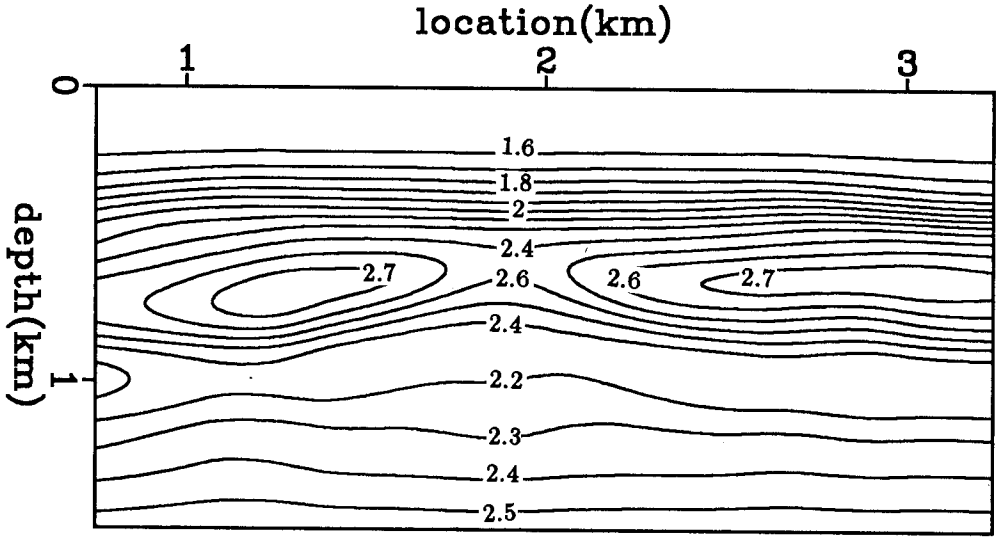

FIG. 3.25. A contour plot of the interval-velocity model obtained after four iterations from the synthetic data. Contour labels are velocities in km/sec.

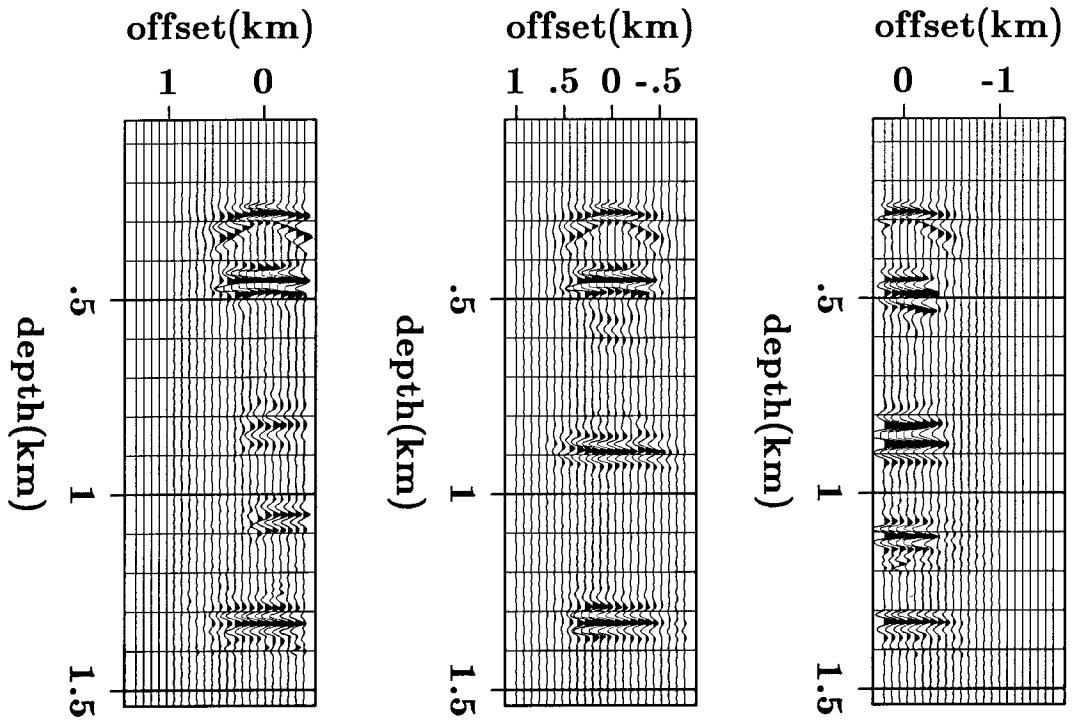

FIG. 3.26. Some post-migration CRG's obtained from the synthetic profiles migrated with the velocity model in Figure 3.25.

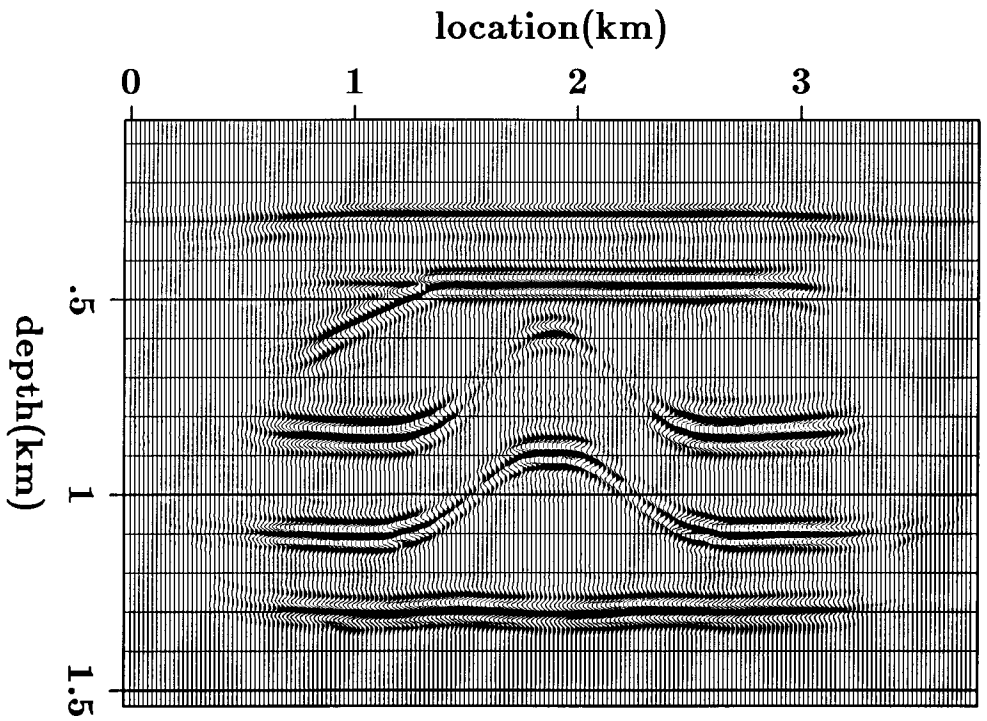

FIG. 3.27. The image obtained by migrating the synthetic profiles with the velocity in Figure 3.25 and stacking.

3.7 SUMMARY

In this chapter, I obtained an interval-velocity model (or interval-slowness model) after migration with a preliminary velocity model. The problem was formulated so that constraints can be put on the interval-velocity model. The method proposed in this thesis was applied to marine and synthetic data sets. The process was terminated when events in the post-migration CRG became aligned horizontally. Using the principle explained in Chapter 2, this alignment means that the velocity used in migration is close to the velocity of the medium. I have also shown that in each iteration the data need to be migrated from scratch.